



Analysis of Insulation Diagnosis for Generator-Motor Stator Winding in Pumped Storage Power Plant

Soo-Hoh Lee¹ · Tae-Sik Kong¹ · Hee-Dong Kim¹

Received: 5 April 2019 / Revised: 6 December 2019 / Accepted: 18 February 2020 / Published online: 20 March 2020
© The Korean Institute of Electrical Engineers 2020

Abstract

In this study, insulation diagnostic tests were conducted on pumped storage power plant (PSPP) generator-motor stator bars with artificially simulated defects in order to improve solutions to perform preventive maintenance and track insulation diagnostic data for generator-motors by proving the effectiveness of insulation indices. Moreover, ozone (O₃) concentration was estimated in order to relate it to partial discharge (PD) in laboratory to ensure the effectiveness of ozone as another index for insulation deterioration. By performing an offline PD test and ultraviolet (UV) observation on one of the generator-motors during overhaul, and an ozone concentration measurement for the identical machine after the overhaul, it was concluded that ozone estimation could be a powerful index for insulation diagnosis under actual operational conditions. It was further developed that ozone measurement is useful to detect not only discharges in slots as mentioned in some studies but also discharges at the end-winding as proven in this study. The findings of this study are expected to contribute to more reliable maintenance of generator-motors in PSPPs by achieving elaborate insulation diagnosis via multiple diagnostic indices.

Keywords Generator-motor · Insulation · Ozone · Partial discharge · Pumped storage power plant · Ultraviolet

1 Introduction

Pumped storage power plants (PSPPs) in South Korea were first constructed in the 1980s to improve system reliability in accordance with the rapid growth of electric power demand. Since the operation of a 400-MW (two 200-MW generator-motors) power plant in 1980, a total of 16 units are currently operational with a maximum power generation capacity of 4700-MW. The fluctuation of the base load is expected to increase owing to South Korea's recent renewable energy expansion policy; hence, the number of PSPPs is expected to steadily increase in order to ensure system reliability. Consequently, a more severe stress is applied to the generator-motor possibly leading to a dielectric breakdown during operation. A sudden dielectric breakdown cannot be

recovered in a short period of time; it lowers the reliability of the electric power supply and causes considerable economic loss. Especially, generator-motors in a PSPP have a characteristic of reaching the rated output in a short period of time after starting. Moreover, it operates under severe operating conditions compared to nuclear or thermal power generators owing to rapid fluctuations and frequent starts and stops depending on the power system conditions.

According to a CIGRE report, 56% of the failures are caused by insulation damage in hydroelectric plants, and among them, 68% are generator stator winding failures [1]. Therefore, preventive maintenance and tracking insulation diagnostic data of generator-motors on a regular basis is important. Besides conventional electrical insulation diagnosis such as estimation of insulation resistance, polarization index, dissipation factor, AC current and partial discharge as described in references [2, 3], various studies have been conducted on the effectiveness of ozone measurement in insulation diagnosis in generators [4, 5]. In reference [4], the relation between partial discharges in slot and ozone production was studied in laboratory and several cases in two power plants were investigated. In reference [5], those relations in slots were also dealt with and electrical and thermal degradation mechanism of stator winding of an air-cooled

✉ Hee-Dong Kim
hdkim90@kepco.co.kr
Soo-Hoh Lee
leesoohoh@kepco.co.kr
Tae-Sik Kong
tskong@kepco.co.kr

¹ Power Generation Laboratory, Korea Electric Power Corporation (KEPCO) Research Institute, Daejeon, Korea

generator was revealed. The usefulness of UV observations of terminal stator windings in high-voltage motors in laboratories was studied in reference [6]. In this paper, to study this notion further, artificially defected bars were fabricated using currently used insulation material and then tested. Furthermore, the usefulness of other diagnostic tools such as ozone measurements and UV observation besides electrical insulation diagnosis was verified on a real generator-motor in PSPP. The motivation for this study is to investigate the possibility to further develop chemical diagnostic methods (ozone measurement) for not only stator winding insulations in slots as mentioned in previous researches but also end-winding insulations to enhance the reliability of online condition monitoring of generator-motor without undergoing interference by surrounding electrical noise.

Several insulation diagnostic tests were performed to assess the insulation quality of three types of artificial defect-introduced stator bars simulating the typical types of breakdown caused by insulation deterioration in actual 18-kV generator-motor stator windings in PSPP applications. Ozone concentration was measured to figure out the relations between ozone and the partial discharge under laboratory conditions. Furthermore, a comprehensive interpretation was made from various diagnostic tests performed before and after insulation refurbishment on one of the generator-motors in Korea to prove the effectiveness and advantage of ozone concentration and UV monitoring will be discussed as a measure to enhance the reliability of insulation diagnosis.

2 Construction of Experimental Specimens

Some studies designed the size, position and shape of artificial voids in insulation system to fabricate experimental samples. However, this is limited to fabricating a single void or several voids which are easy to build. On the other hand, in the case of fabricating voids in the stator winding by adopting actual manufacturing process, massive numbers of voids and various shapes of voids are made at a time. Therefore, as shown in reference [7], the thing that can be controlled for the fabrication and preparation of experimental sample bars is the concept of types of defects and different processes to make the defects. Moreover, the occurrence of electrical discharge is non-linear and dependent on electron production probability. That's why other literatures which manufactured simulated defected bars of massive voids, specify not the size, location, and shape of artificial defects but how to make defects. Although the insulation diagnostic tests are performed on these artificial bars after fabrication, the information that can be drawn from the test results is about the PD pattern, maximum PD magnitude and number of voids by PD tests. If the analysis of the voids by

Scanning Electron Microscope (SEM) is conducted, then the information on the size, position, and shape of voids can be found. However, this is usually done after fabrication, not at a design stage and beyond the limitations of this study. Construction of experimental specimens for this study is illustrated as follows.

First, two sets of 18-kV bars were fabricated via a high-quality manufacturing process identical to that used for standardized ones (Type-D bars). The cross-section of a glass coil was shaped to be 5.9-mm wide and 1.7-mm long in size, and a total of 26 coils were stacked to form one turn. Inner corona-preventive tape was applied around the stacked glass coils and epoxy-mica tape were wound on the top of the inner corona-preventive tape for withstanding electrical stresses on groundwall insulation. To prevent partial discharge on bar surfaces, outer corona-preventive tape (semi-conductive tape) was applied around the groundwall insulation. The cross-sectional size of one turn was 20.0-mm wide and 55.7-mm long. The axial length of each stator bar was 2380.0 mm, including both sides of the end parts. The sectional view of these bars under a well-controlled manufacturing process is expressed in Fig. 1. Moreover, 360° transposition was applied in the same figure during the manufacturing process to simulate actual generator-motor stator bars in PSPPs. This transposition takes the strands and rotates them from the top of the bar to the bottom and back again across the length of the core. In reference [8], thermal phenomena and their effects on operational stability were studied. As a result of this study, it was found that one of the effective ways to relieve stator copper loss was to transpose stator strands. This effectively reduces the flux linking any pair of strands to zero and eliminates the circulating current.

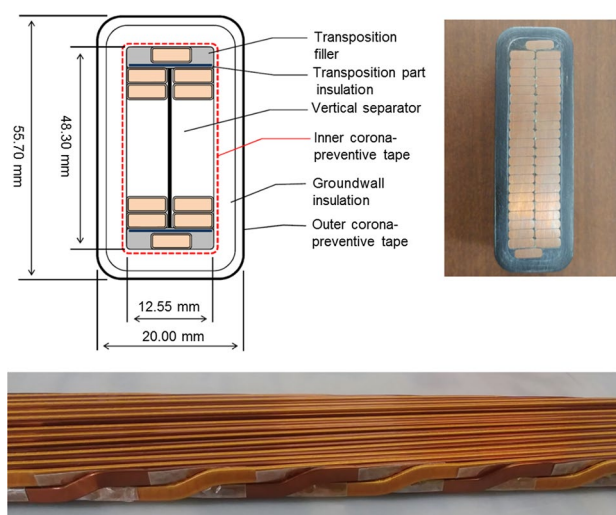


Fig. 1 Sectional view of Type-D bars (upper); 360° transposition applied during the manufacturing process (lower)



Fig. 2 Manufactured bars with sparsely wound outer corona-preventive tape (Type-C bars)

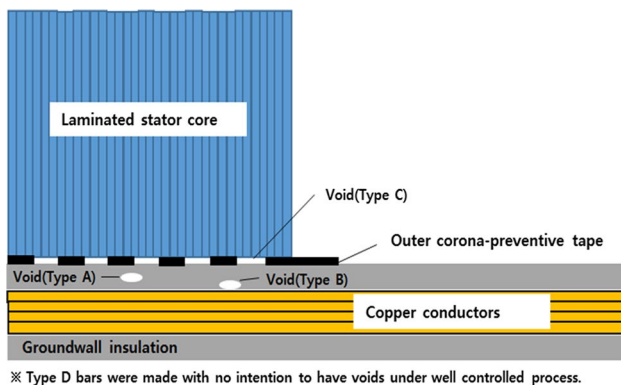


Fig. 3 Fabrication of defected bars

Second, another set of bars were manufactured with an additional layer of Teflon tape in the layers of the groundwall insulation. The Teflon tape was intentionally introduced to produce large artificial voids within groundwall insulations owing to different contraction properties during the heating process. To effectively introduce internal voids for this type of bars (Type-A bars), an additional rapid cooling process after heating at 150 °C for 4 h was applied, unlike other type of bars. Third, two other bars were designed to have voids between the conductors and the groundwall insulations by eliminating inner corona-preventive tapes (Type-B bars). Finally, outer corona-preventive tapes were sparsely wound spaced at 8-mm intervals along the straight portion of the other two bars (Type-C bars) to shape artificial gaps between the groundwall insulation and the iron core, as shown in Fig. 2. The concept of fabricating defected bars as explained above is shown in Fig. 3.

As a whole, four cases of generator-motor stator bars were placed in the slots of the specially designed stator core that can accommodate a maximum of 10 bars at a time with lamination of 1.6-mm-thick steel on a movable carrier, as shown in Fig. 4, to simulate internal discharge (Type-A, 2



Fig. 4 Stator core with inserted bars on a carrier

Table 1 Classification of bars

| Classification of bars | Type of defects | Remarks |
|------------------------|-----------------------------|--------------------------|
| A1, A2 | Internal discharge | Defect simulated process |
| B1, B2 | Discharge from delamination | |
| C1, C2 | Slot discharge | |
| D1, D2 | Internal discharge | Standardized process |

sets), discharge from the delamination of the groundwall insulation from the conductor (Type-B, 2 sets), slot discharge (Type-C, 2 sets), and well processed ones (Type-D, 2 sets). The sets of bars were named A, B, C, and D to stand for the type of defects as listed in Table 1.

3 Experimental Procedure

DC insulation diagnostic tests such as insulation resistance (IR) and polarization index (PI) were conducted on all eight stator bars to observe whether the bars have fundamental strength against an AC high-voltage test. The PI value was obtained by the ratio of IR at 10–1 min, after measuring IR at 1 min using DC Megger (KEW3128, KYORITSU) at a DC voltage of 5-kV at an ambient temperature of 26 °C and humidity of 45%.

After conducting DC insulation diagnostic tests, AC insulation diagnostic tests such as dissipation factor (DF) and AC leakage current were measured to compare the overall characteristics of the insulation of the bars with and without artificial defects. The DF and AC leakage current were measured by applying a 60-Hz AC voltage up to 13 kV (phase voltage $\times 1.25$). A high-voltage supply and control system, Schering Bridge (MIDAS 2880, Haefely)

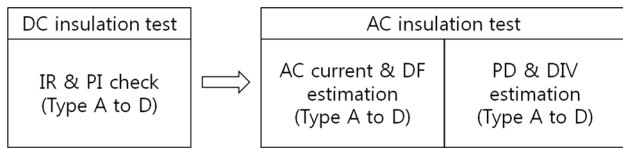


Fig. 5 Block diagram of test procedure

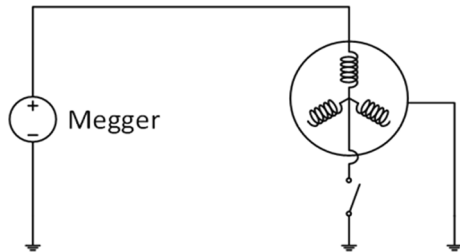


Fig. 6 Circuit diagram for IR and PI test

Table 2 IR and PI test results

| Types of bars | IR [GΩ] | | | | PI |
|---------------|---------|--------|--------------------|--------|------|
| | 26 °C | | 40 °C (Conversion) | | |
| | 1 min | 10 min | 1 min | 10 min | |
| A1 | 243 | 4050 | 92 | 1535 | 16.7 |
| A2 | 384 | 3200 | 146 | 1213 | 8.3 |
| B1 | 391 | 3450 | 148 | 1307 | 8.8 |
| B2 | 422 | 1140 | 160 | 432 | 2.7 |
| C1 | 262 | 537 | 99 | 203 | 2.1 |
| C2 | 542 | 1880 | 205 | 712 | 3.5 |
| D1 | 292 | 4980 | 111 | 1887 | 17.0 |
| D2 | 338 | 4760 | 128 | 1804 | 14.1 |

was used to measure DF and AC currents. The test was conducted at an ambient temperature of 26 °C and humidity of 44%.

Finally, offline partial discharge (PD) was recorded by applying a 60-Hz AC voltage at 10.4 kV (phase voltage) to observe the maximum PD magnitude and its pattern. This was observed using a PD detector (LDS-6, Doble) along with a coupling capacitor (1000 pF). For further study, ozone concentration was measured by applying a 60-Hz AC voltage up to 15.0 kV on Type-C bars using an ozone monitor (Model 202, 2B technologies). This test procedure is shown in Fig. 5.

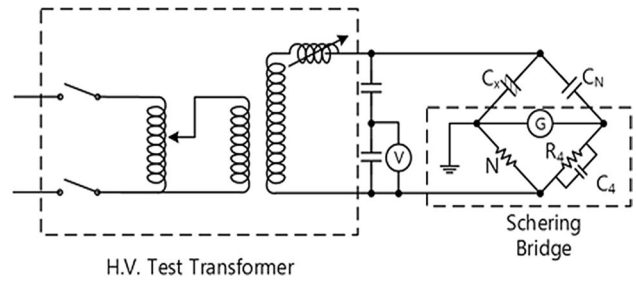


Fig. 7 Circuit diagram for DF estimation

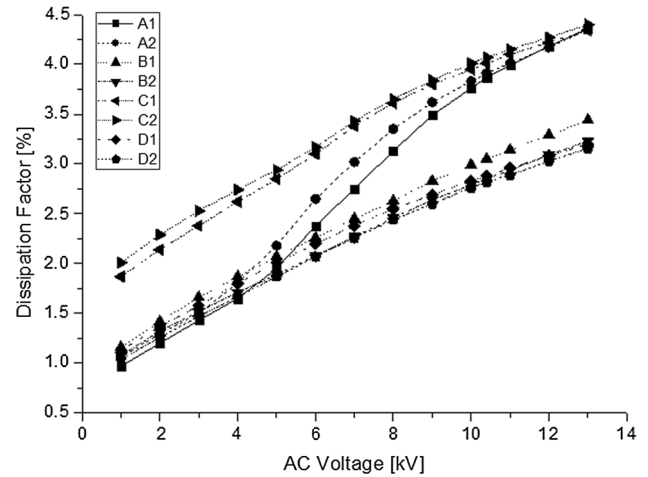


Fig. 8 Characteristics of DF vs. AC voltage

Table 3 DF and Δtanδ of each type

| Voltage [kV] | DF [%] | | | |
|--------------|-----------|-----------|-----------|-----------|
| | A1/A2 | B1/B2 | C1/C2 | D1/D2 |
| 2.0 | 1.20/1.30 | 1.42/1.32 | 2.14/2.29 | 1.37/1.26 |
| 13.0 | 4.36/4.35 | 3.44/3.23 | 4.34/4.40 | 3.20/3.16 |
| Δtanδ | 3.16/3.05 | 2.02/1.91 | 2.20/2.11 | 1.83/1.90 |

4 Test Result and Discussion

The IR and PI values are measured before the AC high-voltage test depending on the circuit diagram of Fig. 6 to ensure that the stator insulation is dry and clean enough to apply high-voltage AC. From the IR and PI test results summarized in Table 2, the test values are seen to meet the standard criteria of IEEE Std. 43 when those were converted from 26 to 40 °C. (IR ≥ 100 MΩ, PI ≥ 2) [9]. Therefore, it was concluded that the dielectric strength against high-voltage AC was sufficient for all eight stator bars.

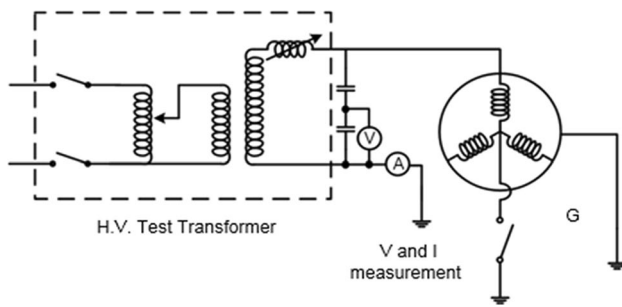


Fig. 9 Circuit diagram for AC current estimation

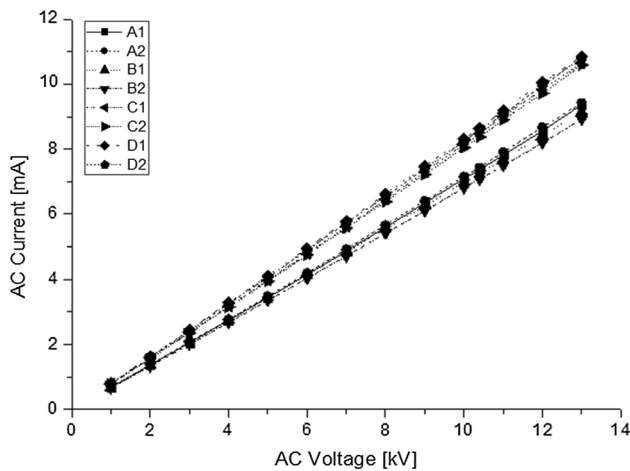


Fig. 10 Characteristics of AC current vs AC voltage

4.1 Estimation of Dissipation Factor (DF)

The circuit diagram of estimation of the dissipation factor (DF) is showed in Fig. 7. The value of DF was measured while increasing the AC voltage from 1 to 13 kV with a step size of 1 kV as shown in Fig. 8, and $\Delta \tan \delta$ was also obtained by subtracting DF at 2 kV from DF at 13 kV (phase voltage $\times 1.25$) as an index for overall insulation deterioration. From Table 3, the value of $\Delta \tan \delta$ was shown to be large in the order of Types A, C, B, and D for both specimens of each type. The largest defect made was observed in the Type-A bar with $\Delta \tan \delta$ values of 3.16 and 3.05 for A1 and A2, respectively. The sharp rise in DF around 5 kV for Type-A bars implies that that an

Table 4 AC current and ΔI of each type

| Voltage [kV] | AC current [mA] | | | |
|----------------|-----------------|-------------|---------------|---------------|
| | A1/A2 | B1/B2 | C1/C2 | D1/D2 |
| 2.0 | 1.369/1.374 | 1.367/1.331 | 1.581/1.569 | 1.630/1.616 |
| 13.0 | 9.362/9.419 | 9.143/8.918 | 10.640/10.590 | 10.850/10.810 |
| I_o | 8.899/8.931 | 8.886/8.652 | 10.277/10.199 | 10.595/10.504 |
| ΔI [%] | 5.21/5.46 | 2.90/3.08 | 3.54/3.84 | 2.41/2.91 |

avalanches of electrical breakdown started at this point. This fact corresponds to discharge inception voltage (DIV) of Type-A bars in Table 5, as shown later. Therefore, DF can be used to check whether there is any PD activity present or not. Apparently, Type-D bars showed the best insulation quality with the lowest values of 1.83 and 1.90 for D1 and D2, respectively.

4.2 Estimation of AC current

The circuit diagram for AC current estimation is shown in Fig. 9. The AC current and ΔI were recorded while increasing the AC voltage from 1 to 13 kV with a step size of 1 kV as shown in Fig. 10. ΔI is obtained from the following equations:

$$\Delta I = (I - I_o) / I_o \times 100\% \tag{1}$$

where I_o denotes the AC current at 13 kV (phase voltage $\times 1.25$) assuming it is proportional to the value at 2 kV.

From the test results listed in Table 4, Type-A bars had the highest value of ΔI for both cases of bars, indicating the largest voids. Type-D bars were in the most-healthy condition recording 2.41 and 2.91 for D1 and D2, respectively, which were the lowest for each specimen. When listing the value of ΔI from the highest to the lowest, the sequence was the same as that of $\Delta \tan \delta$. This indicates that both $\Delta \tan \delta$ and ΔI perform as indices with regard to overall insulation deterioration.

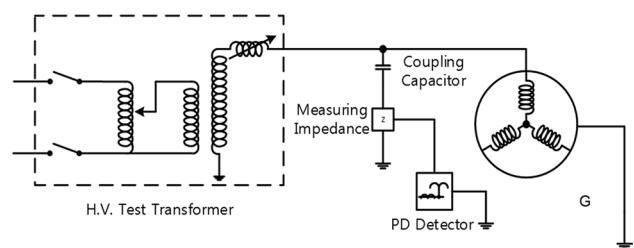


Fig. 11 Circuit diagram for offline PD estimation

Table 5 Offline PD test results

| Types of bars | Discharge inception voltage (DIV) [kV] | Magnitude of PD at 10.4 kV [pC] |
|---------------|--|---------------------------------|
| A1 | 4.5 | 22,110 |
| A2 | 4.8 | 14,653 |
| B1 | 9.0 | 2632 |
| B2 | 9.0 | 2021 |
| C1 | 6.3 | 8063 |
| C2 | 6.5 | 7374 |
| D1 | – | 775 |
| D2 | – | 671 |

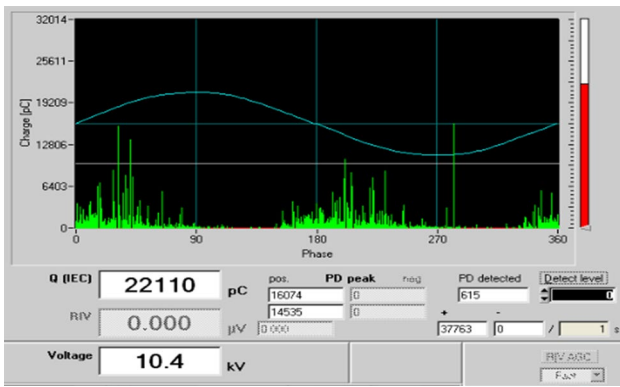


Fig. 12-1 PD magnitude and pattern of Type-A (A1) (22,110 pC at 10.4 kV)

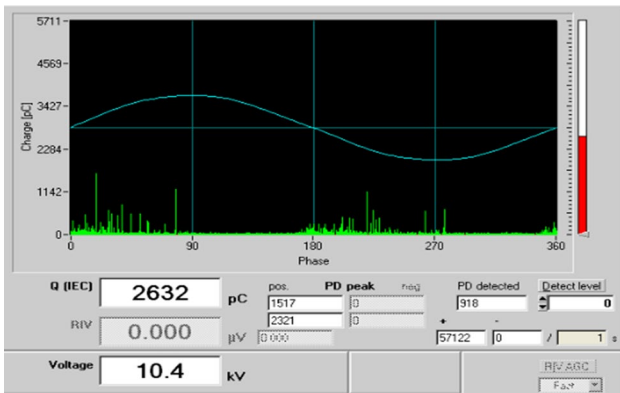


Fig. 12-2 PD magnitude and pattern of Type-B (B1) (2632 pC at 10.4 kV)

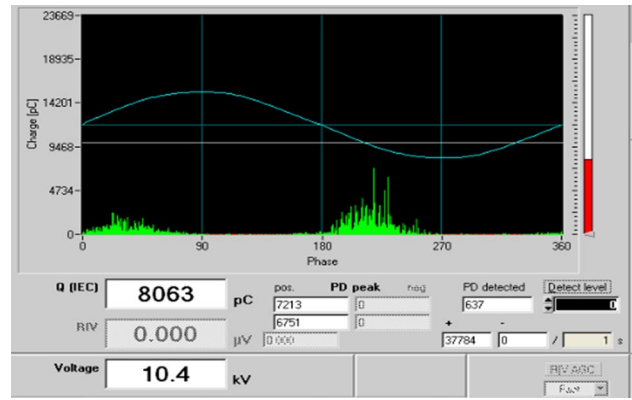


Fig. 12-3 PD magnitude and pattern of Type-C (C1) (8063 pC at 10.4 kV)

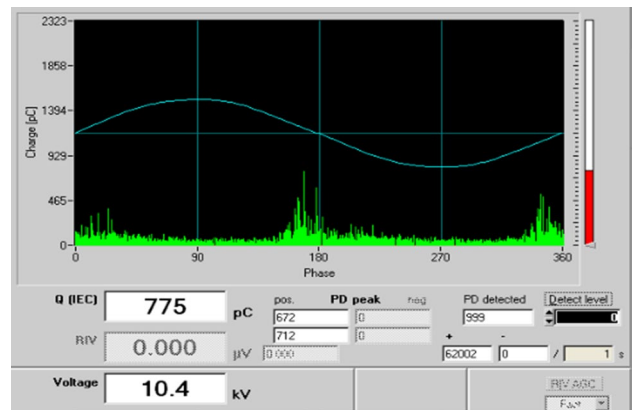


Fig. 12-4 PD magnitude and pattern of Type-D (D1) (775 pC at 10.4 kV)

4.3 Estimation of Offline Partial Discharge (PD)

The circuit diagram of estimation of offline PD is shown in Fig. 11. Unlike $\Delta \tan \delta$ and ΔI which indicate the overall condition of insulations, PD test gives the information

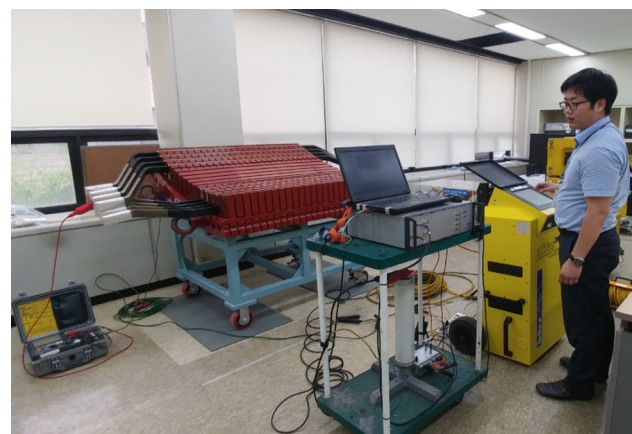


Fig. 13 Conducting offline insulation diagnosis (DF, AC current and PD) on bars with artificial defects

about size of the largest void and its pattern. Offline PD test results are summarized in Table 5. The magnitude of PD was 22,110 pC, 14,653 pC for Type-A, 8063 pC, 7374 pC for Type-C, 2632 pC, 2021 pC for Type-B, and 775 pC, 671 pC for Type-D in the order of magnitude from the highest to the lowest. Definitely, the magnitude of Type-A was by far higher than Type-D by 28.5, 21.8 times for each specimen: A1–D1 and A2–D2. Moreover, the sequence of PD magnitude corresponds to that of $\Delta \tan \delta$ and ΔI . In Figs. 12–1, 12–2, 12–3 and 12–4, the PD magnitude represents the maximum quantity of PD in the insulation of each bar type. Although the PD magnitude is an indicator of how severe the discharge is at the most deteriorated part of the winding, it is related to $\Delta \tan \delta$ and ΔI which are the indicators of the overall condition of winding insulation.

The discharge inception voltage (DIV) was defined at the voltage where 1000 pC is measured. The value of 1000 pC was set to distinguish PD from background noise under laboratory conditions. Note that DIV for the Type-D bars was not recorded because those never reached 1000 pC, indicating that this type of bars were made as the most sound ones as expected. Moreover, the higher the PD magnitude, the lower was the measured DIV. This means that DIV can be a good factor for indicating the deterioration of the insulation of the bars as well. Figure 13 shows how to conduct offline insulation diagnosis on bars with artificial defects in laboratory.

To investigate the PD pattern, the second specimen (A2, B2, C2, and D2) of each type was omitted because it had the same pattern as the first specimen (A1, B1, C1, and D1) for each case. Some features of PD patterns and their interpretation from different sources of discharges were investigated in reference [10, 11]. In reference [10], the PD pattern on four cases for two generators that had dielectric breakdown was studied. And three types of PD patterns and their mechanism were analyzed for high-voltage motors in reference [11]. When referring to these studies, it could be deduced that Type-A and Type-D bars demonstrated typical internal discharge in the groundwall insulation from Figs. 12–1 and

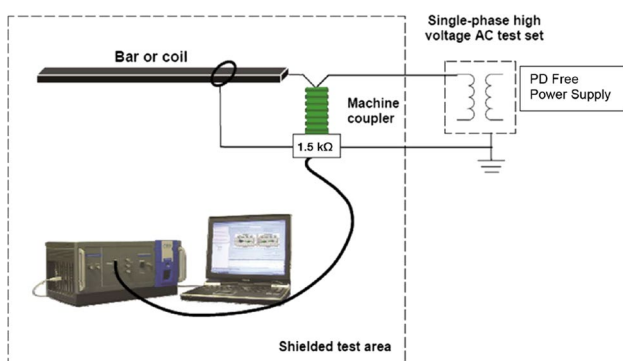


Fig. 14 Schematic for online PD test [12]

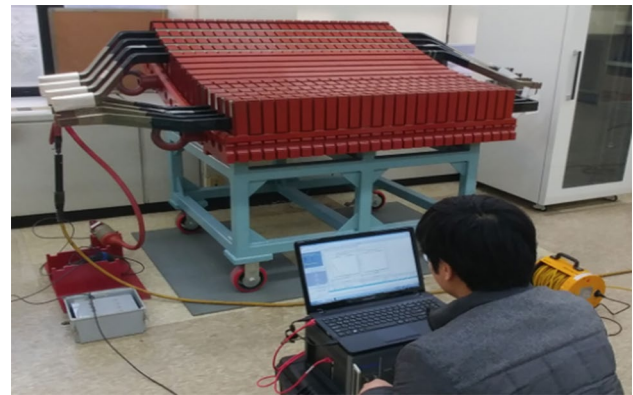


Fig. 15 Performing online PD test

12–4, as expected. In Fig. 12–3, the slot discharge pattern was observed clearly for Type-C. For Type-B, as shown in Fig. 12–2, it seems that the maximum PD magnitude occurred in positive voltage cycle which indicate conductor delamination PD pattern. However, it's difficult to recognize it because the artificial voids between the conductor and groundwall insulation were fabricated into a small size to

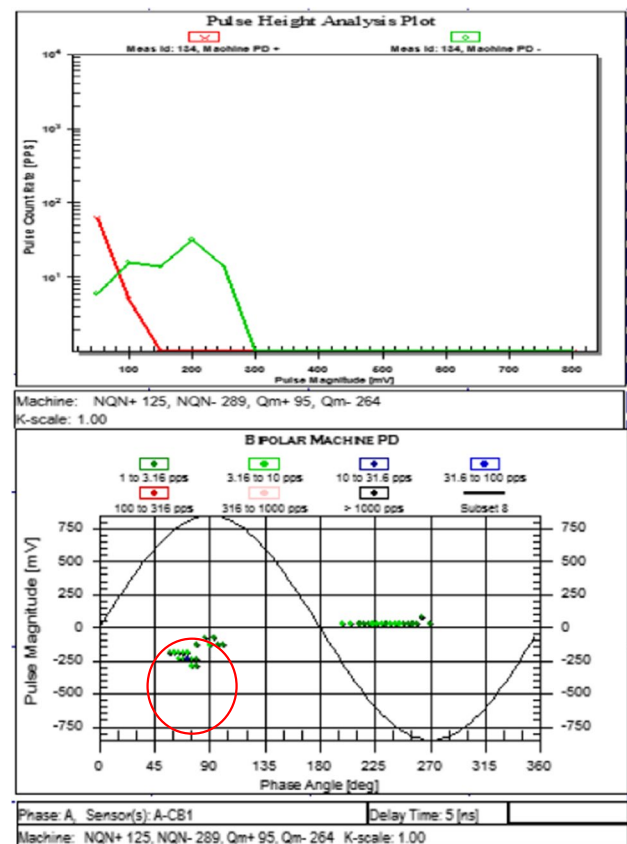


Fig. 16 PD pattern for Type-B1 at 13.0 kV (NQN +:125, NQN -:289, Qm +:95, Qm -:264, Qm-/Qm +:2.78)

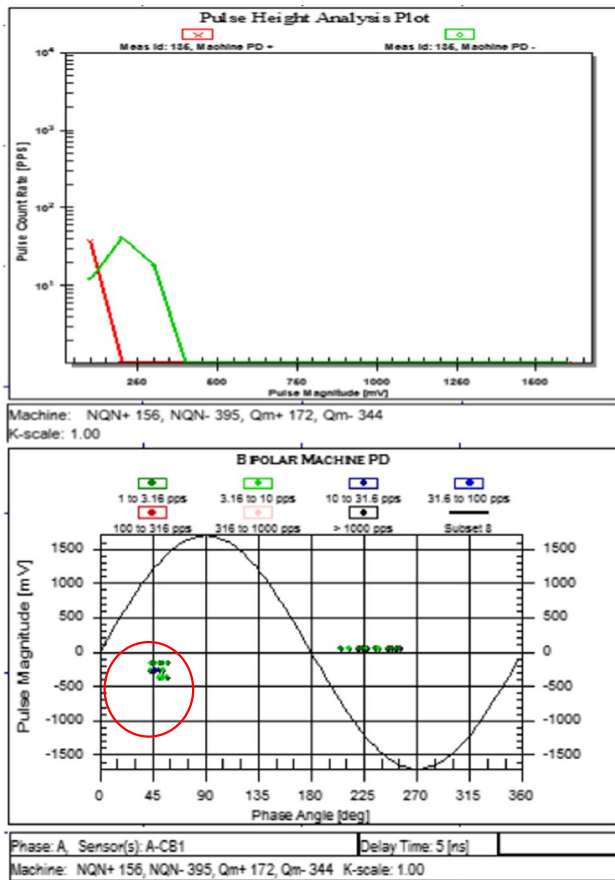


Fig. 17 PD pattern for Type-B1 at 15.0 kV (NQ_N+ :156, NQ_N- :395, Q_m+ :172, Q_m- :344, Q_m-/Q_m+ :2.00)

distinguish it from internal discharge PD pattern. Furthermore, Roebel bars with epoxy-mica insulation tend to be rarely affected by delamination at the conductor-insulation interface [7]. Therefore, additional work was performed using an online PD detector (TGA-B, IRIS) with a 80-pF coupling sensor, as shown in Figs. 14 and 15, to further study the PD pattern for Type-B.

4.4 Estimation of Online PD

Recommendations were provided for testing of sample coils to obtain a better quality form-wound stator winding in reference [12]. When referring to sample coil test method in [12], the schematic for the estimation of online PD to detect void in stator bar insulation is described in Fig. 14. For this test, an online PD detector (TGA-B, IRIS) and Coupling Capacitor of 80-pF were set up as shown in Figs. 15, 16 and 17 show the result of the PD distribution for Type-B1 when applying an AC voltage higher than the phase voltage, namely at 13.0 kV and 15.0 kV. From the test results, it was obvious that the maximum partial discharge occurred in 45°–90° phase and had the discharge pattern of conductor

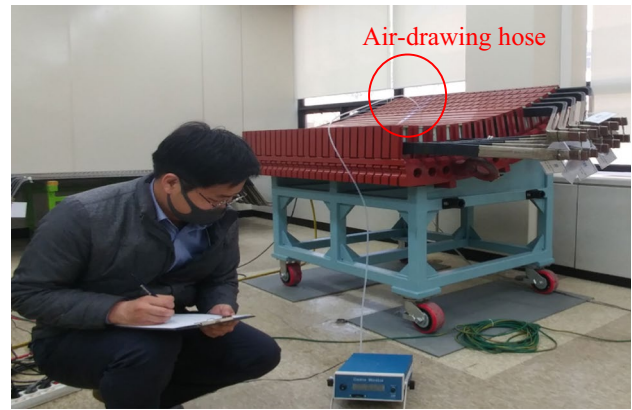


Fig. 18 Ozone estimation of Type-C bars

delamination based on the ratio of Q_m- to Q_m+ : 2.78, 2.00 at 13.0, 15.0 kV, respectively. In reference [13], two cases of online PD measurements for gas turbine generators were analyzed. And online PD measurement data in hydrogen-cooled generators were investigated in reference [14]. When considering the PD pattern from those studies, it was concluded that Type-B bars have the PD pattern of delamination at the conductor–insulation interface.

4.5 Relationship Between PD and Ozone (O₃)

The schematic diagram for ozone measurement is identical to Fig. 9 except for the installation of the ozone monitor while applying 60 Hz AC voltage up to 15.0 kV on Type-C bars. An ozone monitor (Model 202, 2B technologies) was used to record the data every 10 s with the air-drawing hose placed in the middle of the core through the air duct, as shown in Fig. 18, under an ambient temperature of 26 °C and humidity of 48%.

Ozone was not estimated for the Type-A, Type-B, and Type-D bars when applying AC high voltage because ozone is produced when slot discharge occurs. It is obvious that bars for Type-A, Type-B, and Type-D

Table 6 Relation between PD and O₃ (Type-C)

| Type of bars | Voltage | | |
|----------------------|---------|---------|---------|
| | 10.4 kV | 13.0 kV | 15.0 kV |
| C1 bar | | | |
| O ₃ [ppb] | 952 | 1850 | 2240 |
| PD [pC] | 8063 | 12,819 | 13,687 |
| O ₃ /PD | 0.118 | 0.144 | 0.164 |
| C2 bar | | | |
| O ₃ [ppb] | 722 | 1512 | 1976 |
| PD [pC] | 7374 | 9723 | 11,072 |
| O ₃ /PD | 0.098 | 0.156 | 0.178 |



Fig. 19 Ozone monitoring in the generator-motor room

have voids inside the insulations while bars Type-C have voids between the insulations and core. Furthermore, the insulation of Type-C bars is directly exposed to the air. Therefore, it can be concluded that bars for Type-C produce massive ozone when applying the AC high voltage at 10.4, 13.0, and 15.0 kV. Noting that the corona progresses when ozone occurs, corona phenomenon was observed using a UV camera (Model Luminar, OFIL) in the laboratory. However, it was turned out that the occurrence of corona emission was not enough to recognize it because it occurred inside the core ducts. Instead, UV observation was conducted at the visible end-winding in a real generator-motor as shown later in Fig. 22. Further discussion will be made in 4.6.

Table 6 shows the test results, from which the following information can be deduced. Firstly, it was found that PD and ozone are positively related in case of slot discharge, and the ratio of PD to O_3 ranges from 0.118 to 0.164 for the C1 bar and 0.098 to 0.178 for the C2 bar. These ratios are meaningful because, unlike for Type-C bars, those for other types of bars (Type-A, Type-B, and Type-D) nearly converge to zero.

Secondly, the ratio of PD to O_3 increases when applying higher voltages in steps of 10.4, 13.0, and 15.0 kV because the ozone concentration is likely to be more saturated in a higher voltage.

4.6 Advantage of Ozone Monitoring in PSPP

To prove the effectiveness of ozone monitoring in real PSPP, the ozone concentration was measured for ten air-cooled generator-motors in Korea. The ozone estimation procedure was identical to that followed in the laboratory, with

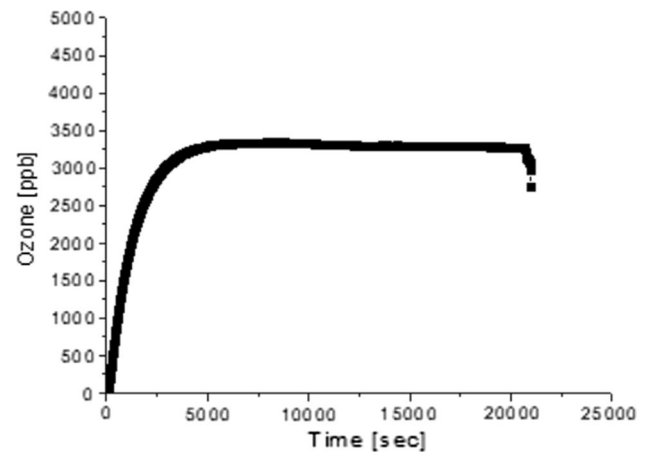


Fig. 20 Ozone measurements in 'A' PSPP

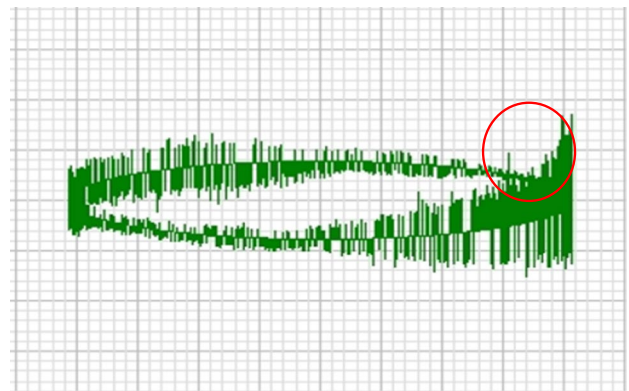


Fig. 21–1 PD measurement before insulation refurbishment (36,260 pC at 10.4 kV, Phase A)

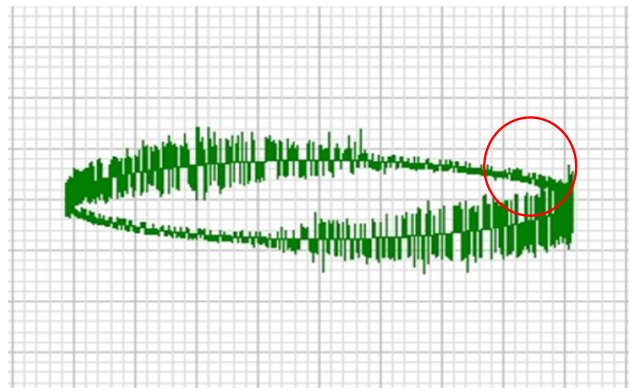


Fig. 21–2 PD measurement after insulation refurbishment (10,676 pC at 10.4 kV, Phase A)

the exception that the air-drawing hose was placed inside a generator-motor room to draw ventilating air. Figure 19 shows the ozone concentration measurement inside one of the generator-motor rooms.

It was found that one of the PSPPs ('A' PSPP) had a significantly higher ozone concentration while that of the others was within the normal indoor range of 10–20 ppb. From the ozone concentration monitoring, it was found that, at rated 18 kV applied under an ambient temperature of 16 °C and humidity of 22%, the 'A' PSPP was saturated to an average of 3400 ppb after 1.5 h after it had started, as shown in Fig. 20.

Before ozone measurement, this machine had been diagnosed to have a pattern of slot discharge, as shown in Fig. 21–1. Damage to the semi-conductive layer on the stator winding and winding wear was suspected. Therefore, during the overhaul 2 months before the ozone measurement, insulation refurbishment of stator windings was conducted including replacement of unstable slot wedges, application of insulating paint and varnish on the worn semi-conductive tape on bars near core slots, and replacement of end-winding binding. Figure 21–2 shows PD test results after insulation refurbishment. Significant reductions were apparent on the magnitude from 36,260 to 10,676 pC as well as on the pattern of slot discharge in the 180°–225° phase after insulation refurbishment.

Additionally, the occurrence of corona was observed at the stator end-winding using a UV camera (Luminar, OFIL). The result showed that the 13,226 pulses were recorded from the PD when applying a phase voltage of 10.4 kV, as shown in Fig. 22. Therefore, it was concluded that the slot discharge due to loose bars was reduced, but discharges at the end winding still existed after insulation refurbishment.

The results of the above offline PD test, UV observation, and ozone measurement showed that in spite of significant reduction in the occurrence of slot discharge after insulation refurbishment, the ozone was still significantly higher than in other generator-motors when measured 2 months after insulation refurbishment. It was concluded that this high concentration of ozone was caused from inadequate end-winding spacing and silicon carbide coating deterioration based on the UV observation at the stator end winding.

Therefore, ozone estimation is a useful index to diagnose not only semi-conductive coating deterioration but also the condition of end-winding in case of surface discharge in an air-cooled machine. Furthermore, it does not undergo interference by surrounding electrical noise and is easy to perform even during the operation of a generator-motor. When diagnosing the condition of the insulation, it is necessary to periodically track the trend of ozone data for an identical machine because ozone concentration is dependent on the cooling air velocity of the generator-motor and the position of the air-sucking sensor of the ozone monitor. It was reported that the ozone concentration is dependent on not only the voltage applied and air velocity of ventilation but also the humidity in reference [15]. The effect of humidity and seasonal weather conditions on ozone concentration is

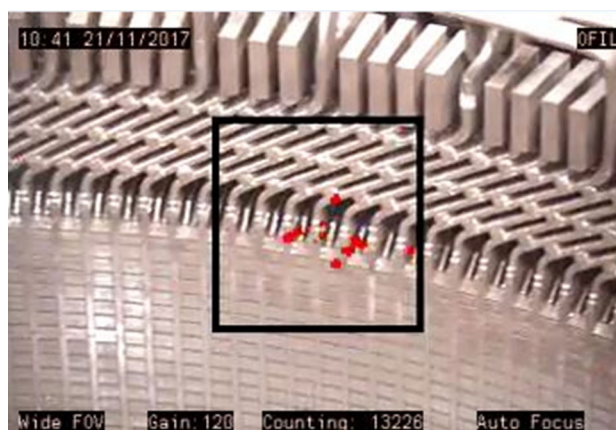


Fig. 22 UV observation (13,226 counting at 10.4 kV, Phase A, Gain: 120)

beyond the limit of this study and needs to be study further later.

It was also found that UV observation is an effective tool for insulation diagnosis during overhaul because it can visually detect discharges at the exact damaged spot of end-winding which cannot be done by the offline PD test.

5 Conclusion

In this study, insulation diagnostic tests were performed on three types of bars with artificial defects (6 sets) in comparison to bars under standardized manufacturing process (2 sets) for 18-kV generator-motors in PSPP. An offline PD test and a UV observation were performed on one of the generator-motors during overhaul. Moreover, ozone concentration was measured for the identical machine after the overhaul to prove the expanded effectiveness of ozone monitoring during operation. The conclusions drawn from a comprehensive analysis of the test results can be summarized as follows.

First, it was shown that electrical indicators ($\Delta \tan \delta$, ΔI , PD magnitude, DIV) for insulation deterioration were consistent with each other and worked efficiently. When listed in order from the highest to the lowest, the values of $\Delta \tan \delta$ and ΔI had the same sequence as the PD magnitude representing the maximum size of void: Type-A, Type-C, Type-B, and Type-D from the highest to the lowest. Moreover, the lower the DIV, the higher the $\Delta \tan \delta$, ΔI , and PD magnitude.

Second, the PD patterns were observed as expected. An internal discharge pattern was found on the Type-A and Type-D bars and a slot discharge pattern was shown on the Type-C bars. For Type-B bars, additional PD monitoring system was set up to ensure the PD pattern by stepping up the voltage over the rated voltage; the result was positive in terms of its pattern of conductor delamination.

Third, an additional chemical index (O_3) was developed by correlating it with the PD data for Type-C bars. Furthermore, the ozone concentration was measured and analyzed in detail for one of the generator-motors in PSPP in Korea to ensure the expanded effectiveness and advantage of ozone monitoring on insulation diagnosis not only in case of slot discharges but also discharges at end-winding as proven in this study. It is beneficial to track down ozone data recorded at a designated place for an identical air-cooled generator-motor to deduce its transition to insulation deterioration especially in terms of surface discharge. However, it still needs to study further the effect of weather conditions on the trend of ozone concentration combined with online PD pattern. Nevertheless, it is definite that the ozone measurement is relatively easy to perform because it can be conducted during normal operation. Above all, it has a strong advantage of rarely undergoing interference from the electrical noise from surrounding facilities.

Finally, the usefulness of UV observation with an offline PD test was also found. Like ozone measurements, it does not undergo interference from the electrical noise. The ease of its application and the visualization of damaged parts of the end-winding are unique advantages that conventional PD tests cannot provide; offline PD can detect insulation deterioration in slots rather than at the end-winding.

In conclusion, it is expected that more sophisticated preventive maintenance will be realized by a comprehensive interpretation through electrical insulation diagnosis by indicators such as $\Delta \tan \delta$, ΔI , PD magnitude, and its pattern along with UV observation during overhaul. There were some limitations of this study regarding the effect of humidity on ozone concentration. This needs to be studied further by correlating the ozone concentration with online PD data under different weather conditions. In spite of this limitation, it is definite that ozone monitoring are expected to be helpful for operators to detect insulation deterioration and respond at an early stage of possible failure of generator-motors in PSPP.

References

1. CIGRE Study Committee SC11, EG11.02 (2003) Hydrogenerator failures-result of the survey
2. IEC Standard (2011) Evaluation and qualification of electrical insulation systems. IEC Std. 60505
3. IEEE Standard (2014) IEEE guide for the measurement of partial discharges in AC electric machinery. IEEE Std. 1434–2014
4. Lépine L, Lessard-Déziel D, Bélec M, Guddemi C, Nguyen DN (2007) Understanding ozone distribution inside stator core and measurements inside air-cooled generators to assess partial

5. Bélec M, Li S, Nguyen DN, Lépine L, Guddemi C, Lessard-Déziel D, Schwartz T, Lamarre L (2007) Investigation and diagnosis of a 184-MVA air-cooled generator heavily affected by slot partial discharge activity. In: Electrical Insulation Conference and Electrical Manufacturing Expo. Nashville, USA
6. Kong T-S, Kim H-D, Lee S-H, Lee J (2017) Analysis of correlation among partial discharges, ozone emission, and UV radiation in HV motor stator windings. *Am J Electr Power Energy Syst* 6(6):113–118
7. Hudon C, Bélec M (2005) Partial discharge signal interpretation for generator diagnostics. *IEEE Trans Dielectr Electr Insul* 12(2):297–319
8. Stein J (2011) Generator Stator Endwinding Vibration Guide: Tutorial. EPRI(TR): Palo Alto, 1021774
9. IEEE Standard (2013) IEEE recommended practice for testing insulation resistance of electric machinery. IEEE Std. 43
10. Kong T-S, Kim H-D, Park T-S, Kim K-Y, Kim H-Y (2015) Analysis of partial discharge patterns for generator stator windings. *Am J Electr Power Energy Syst* 4(2):17–22
11. Wang W, Yan L, Wang T, Yu H, Han Y, Liu X, Zhang N, Wu N (2016) PD mechanism and pattern investigation for stator winding insulation of HV motors. In: Proceedings of 2016 IEEE International Conference on Mechatronics and Automation, Harbin, China
12. Johnson W (2014) Guide for sample stator coil inspection and testing during motor rewinds and manufacturing. EPRI (TR), 3002003261
13. Kim H-D, Kong T-S, Park T-S, Son T-h (2014) Analysis of on-line partial discharge trend in gas turbine generators. *Int J Energy Power* 3(3):42–48
14. Stone GC, Chan C, Sedding HG (2016) On-line partial discharge measurement in hydrogen-cooled generators. In: 2016 IEEE Electrical Insulation Conference, Montréal, Canada
15. Gray D (2001) Hydro life extension modernization guide. EPRI(TR), 112350-V3

Publisher's Note Springer Nature remains neutral with regard to jurisdictional claims in published maps and institutional affiliations.



Soo-Hoh Lee received his B.S. degrees in Electrical Engineering from Kyungbook National University, Daegu, Korea in 2010, and M.S. degree in Design of Wind Turbine Generator from POSTECH, Pohang, Korea in 2012. He worked for the Department of Rotating Machinery Development, Hyundai Heavy Industry from 2012 to 2016. Since 2016, he has been working for the Korea Electric Power Corporation (KEPCO). He is currently a senior researcher with the Technical Experts

Center, Power Generation Laboratory, KEPCO Research Institute, Daejeon, Korea.



Tae-Sik Kong received his B.S. degrees in Electrical Engineering from Chungbuk National University, Cheongju, Korea, in 1997, and M.S. degree in Electrical Engineering from Chungnam National University, Daejeon, Korea in 2004. Since 1997, he has been working for the Korea Electric Power Corporation (KEPCO). He is currently a principal researcher with the Technical Experts Center, Power Generation Laboratory, KEPCO Research Institute, Daejeon, Korea. His research interests

include diagnostic test and reliability for rotating machines.



Hee-Dong Kim received the B.S, M.S and Ph.D. degrees in Electrical Engineering from Hongik University, respectively. He is currently a chief researcher in the Power Generation Laboratory at Korea Electric Power Corporation (KEPCO) Research Institute. He was a visiting researcher in the Department of Electrical Engineering, Kyushu Institute of Technology, Kitakyushu, Japan. His research interests are rotating machines, diagnostic tests, partial discharge, pulse propagation, electrical

insulation, and continuous monitoring systems.